Fluorescence diffuse optical tomography using upconverting nanoparticles

Can T. Xu,[a] Johan Axelsson, and Stefan Andersson-Engels
Department of Physics, Lund University, P.O. Box 118, S-221 00 Lund, Sweden

(Received 6 May 2009; accepted 29 May 2009; published online 23 June 2009)

Fluorescence diffuse optical tomography (FDOT) can provide important information in biomedical studies. In this ill-posed problem, suppression of background tissue autofluorescence is of utmost importance. We report a method for autofluorescence-insensitive FDOT using nonlinear upconverting nanoparticles ($NaYF_4:Yb^{3+}/Tm^{3+}$) in a tissue phantom under excitation intensities well below tissue-damage thresholds. Even with the intrinsic autofluorescence from the phantom only, the reconstruction of the nanoparticles is of much better quality than the reconstruction of a Stokes-shifting dye. In addition, the nonlinear power dependence leads to more confined reconstructions and may increase the resolution in FDOT. © *2009 American Institute of Physics*. [DOI: 10.1063/1.3156857]

Within the field of biomedicine, a huge interest exists for longitudinal studies of small animals using noninvasive, highly sensitive, and relatively inexpensive systems. During the last few years, fluorescence diffuse optical imaging (FDOI) has been developed to become an excellent tool for this purpose.[1–3] Such a tool could, for example, be used to monitor the drug distribution and targeting on cancer tumors as well as the effects of the drug on the tumors inside a small animal.[3] The increasing interest of FDOI has catalyzed the development of a framework for fluorescence diffuse optical tomography (FDOT).[2,4] FDOT is a powerful inverse method used to reconstruct an internal fluorophore distribution inside a highly scattering material by acquiring the boundary fluence for multiple source-detector pairs. The reconstruction is achieved by fitting the collected boundary data to a model, for example, the diffusion model. However, the problem is often very ill-posed. The ill-posedness of the problem can be slightly alleviated by using large data sets. However, this cannot solve all the problems since the ill-posedness is ultimately a matrix property.[5] It is hence of utmost importance to minimize any noise or background of the collected data. Although much of the noise can be eliminated by employing low-noise equipment, an intrinsic source of background known as the tissue autofluorescence remains to plague the measurements using traditional Stokes-shifting fluorophores.

Autofluorescence is an intrinsic property of an object of interest; it cannot be easily corrected through, for example, background subtraction.[6] Several approaches have been suggested to overcome this issue, with one of the most popular being spectral unmixing.[7] Using spectral unmixing, the data have to be collected for many different wavelength bands, which can be highly demanding in terms of instrumentation and measurement procedure. This approach also generates large amount of data, which may become a computational challenge for the inverse tomographic problem.

Quantum dots have been proposed as fluorophores that are less sensitive to tissue autofluorescence. This has been motivated by the fact that quantum dots can be engineered to emit a signal with a Stokes shift greater than that of the typical tissue autofluorescence. Unfortunately, using quantum dots, the signal is still not autofluorescence free and may still require extensive postprocessing.[8] In addition, quantum dots are often fabricated with heavy metal crystalline cores, which are highly toxic and require protection by, for example, oxide or polymer coatings. However, recent studies have shown that the stability can be compromised in biological environments and the release of highly toxic heavy-metal ions is likely inevitable.[8]

The above mentioned approaches can reduce the effects of tissue autofluorescence but they do not fully eliminate the problem. Upconverting nanoparticles have been proposed as fluorophores that are completely insensitive to tissue autofluorescence. These particles can emit anti-Stokes shifted light upon near-infrared excitation,[9] which enables the signal to be detected in an autofluorescence-free environment. The use of upconverting nanoparticles in deep diffuse tissue imaging has, for some time, been limited by the low quantum efficiency. However, recent advances in technology have greatly enhanced the quantum efficiency of the nanoparticles,[10,11] which have enabled them to be imaged in deep diffuse materials under conservative excitation intensities.[12,13]

All work concerning nanoparticles for biomedical applications on the macroscopic scale to date has been focused on imaging only. In this letter, we demonstrate autofluorescence-insensitive FDOT using $NaYF_4:Yb^{3+}/Tm^{3+}$ upconverting nanoparticles emitting at 800 nm when excited at 980 nm. The experiments were carried out in a controlled environment using a gelatin tissue phantom, in which a comparison of the reconstructed results between upconverting nanoparticles and Rhodamine 6G was made. For all the experiments, the only source of autofluorescence was the intrinsic one from the tissue phantom itself, i.e., no exogenous fluorophores were added to the phantom to simulate autofluorescence.

In this study, the sought parameter in the reconstruction scheme was the fluorophore number density, $\eta(\mathbf{r})$, inside the phantom domain of interest, Ω, using a set of measured fluence rates on the surface, $\partial\Omega$. For the calculations, Ω was discretized into N voxels and the fluorophore number density becomes $\mathbf{n}=[\eta(\mathbf{r}_1),\eta(\mathbf{r}_2),\ldots\eta(\mathbf{r}_N)]^{\mathrm{T}}$. The problem was formulated as an optimization problem by minimizing the residual between the predicted fluorescence fluence rates, $\mathbf{\Theta}_{\mathrm{f}}^{\mathrm{c}}(\mathbf{n})$, in a forward model, and the measured fluence rates,

[a]Electronic mail: can.xu@fysik.lth.se.

$\boldsymbol{\Theta}_{\mathrm{f}}^{\mathrm{m}}$, in an experimental setup. As the minimization problem is ill-posed, Tikhonov regularization was used to single out a useful and stable solution. The regularized solution in $\mathbf{n}$ was found by minimizing the quantity

$$\chi^2 = \|\boldsymbol{\Theta}_{\mathrm{f}}^{\mathrm{c}}(\mathbf{n}) - \boldsymbol{\Theta}_{\mathrm{f}}^{\mathrm{m}}\|_2^2 + \lambda\|\mathbf{I}[\mathbf{n} - \mathbf{n}_0]\|_2^2, \tag{1}$$

where λ is the regularization parameter, explained below, and $\mathbf{n}_0$ is the initial estimate of the fluorophore distribution, which was set to zero for all reconstructions.

The forward fluorescence problem was modeled using two coupled diffusion equations. However, as reported,[13] the emission of the upconverting nanoparticles has a nonlinear dependence on the excitation power, which gives rise to a nonlinear source function $S_{\mathrm{f}}[\Phi_{\mathrm{e}}(\mathbf{r})] = C\Phi_{\mathrm{e}}^{\gamma}(\mathbf{r})$, where C is a constant depicting the efficiency of a fluorophore. For ordinary organic fluorophores, such as Rhodamine 6G, $\gamma = 1$, thus the relation is linear with respect to the excitation fluence rate. For the case of the nanocrystals used in this study, $\gamma = 2$, as the power dependence was determined experimentally to be quadratic.[13] The two coupled diffusion equations can now be written as

$$(\mu_{\mathrm{a}}^{\mathrm{e}} - \kappa_{\mathrm{e}}\nabla^2)\Phi_{\mathrm{e}}(\mathbf{r}) = S(\mathbf{r}), \tag{2}$$

$$(\mu_{\mathrm{a}}^{\mathrm{f}} - \kappa_{\mathrm{f}}\nabla^2)\Phi_{\mathrm{f}}(\mathbf{r}) = \eta(\mathbf{r})C\Phi_{\mathrm{e}}^{\gamma}(\mathbf{r}), \tag{3}$$

where $\mu_{\mathrm{a}}^{\mathrm{e,f}}$ and $\kappa_{\mathrm{e,f}}$ denote the absorption and diffusion coefficients at the excitation and fluorescence wavelengths, respectively. As mentioned above, the measurable quantity was the fluence rate at the surface of the phantom, thus the data function for each source-detector pair in the discretized domain using $\eta'(\mathbf{r}) = \eta(\mathbf{r})C$ was defined as

$$\Theta_{\mathrm{f,(sd)}}^{\mathrm{c}} = \sum_{i=1}^{N} U_{\mathrm{f}}^{*}(\mathbf{r}_{\mathrm{d}}, \mathbf{r}_i)\,\eta'(\mathbf{r}_i)[U_{\mathrm{e}}(\mathbf{r}_{\mathrm{s}}, r_i)]^{\gamma}\Delta V_i, \tag{4}$$

where $\mathbf{r}_{\mathrm{s,d},i}$ denotes the coordinates for source, detector, and voxel, respectively, and ΔV_i is the volume of voxel i. $[U_{\mathrm{e}}(\mathbf{r}_{\mathrm{s}}, \mathbf{r}_i)]^{\gamma}$ represents the forward solution of the excitation light at $\mathbf{r}_i$ with the source positioned at $\mathbf{r}_{\mathrm{s}}$, while $U_{\mathrm{f}}^{*}(\mathbf{r}_{\mathrm{d}}, \mathbf{r}_i)$ represents the adjoint solution to the forward fluorescence problem at $\mathbf{r}_i$ with the detector positioned at $\mathbf{r}_{\mathrm{d}}$.

Since Eq. (4) is linear with respect to the fluorophore distribution and the regularization term in Eq. (1) is quadratic, the fluorophore distribution, using a damped Gauss–Newton method, could be reconstructed directly using the scheme

$$\mathbf{h} = (\mathbf{A}^{\mathrm{T}}\mathbf{A} + \lambda\mathbf{I})^{-1}\mathbf{A}^{\mathrm{T}}(\boldsymbol{\Theta}_{\mathrm{f}}^{\mathrm{c}} - \boldsymbol{\Theta}_{\mathrm{f}}^{\mathrm{m}}), \tag{5}$$

where $\mathbf{h} = \mathbf{n}_0 - \mathbf{n}$ is the update vector and A is a matrix containing the sensitivity profiles with the elements $A_{(sd),i}U_{\mathrm{f},d,i}^{*}C(U_{\mathrm{e},s,i})^{\gamma}\Delta V_i$. For all the reconstructions, λ was initially set to a large value and gradually decreased with a factor of $10^{1/4}$ until two consecutive runs differed by less than 1%.

A solid tissue phantom was prepared with water, gelatin, TiO_2, and ink. The relevant optical properties were measured with a time-of-flight spectroscopy system employing a supercontinuum white-light source. The scheme is similar to the one described in Ref. 14. The optical properties were determined to have a reduced scattering coefficient $\mu_{\mathrm{s}}' = 8.0\ \mathrm{cm}^{-1}$ and an absorption coefficient $\mu_{\mathrm{a}} = 0.29\ \mathrm{cm}^{-1}$ for $\lambda = 660$ nm, which are close to those found in small animals.[15] Fluorescent lesions were simulated through two capillary tubes with inner diameters of 2.4 mm. The first tube was filled with a solution of Rhodamine 6G, $c = 0.1\ \mu\mathrm{M}$, and the second tube was filled with a solution of the nanoparticles, $c = 1$ wt %. The concentrations of the fluorophores were chosen to correspond to the concentrations obtainable in *in vivo* studies.[4,13,16] The experimental setup is schematically shown in Fig. 1. The thickness of the phantom was 17 mm, and the tubes were inserted into the tissue phantom at a depth of 1 cm as shown in upper right of Fig. 1. Excitation of the fluorophores was performed using a 532 nm laser (Viasho VA-I-N-532–200mW, Beijing, China) for the dye and a 980 nm laser (Thorlabs L975P1WJ, Dachau, Germany) for the upconverting nanoparticles. The beams from the lasers were slightly focused to scan the phantom from below. A charge-coupled device (CCD) camera (Andor iXon DU-897, Belfast, Ireland) captured one image for every scanned position through a set of dielectric bandpass filters centered at 800 nm for the upconverting nanoparticles and 600 nm for the dye. The spot size of the lasers was determined to be 0.20 cm^2, giving intensities of 480 $\mathrm{mW/cm}^2$ for the 980 nm laser and 85 $\mathrm{mW/cm}^2$ for the 532 nm laser, which are well below the damage thresholds of continuous human skin exposure. For the reconstructions, 10^4 source-detector pairs were used in this work.

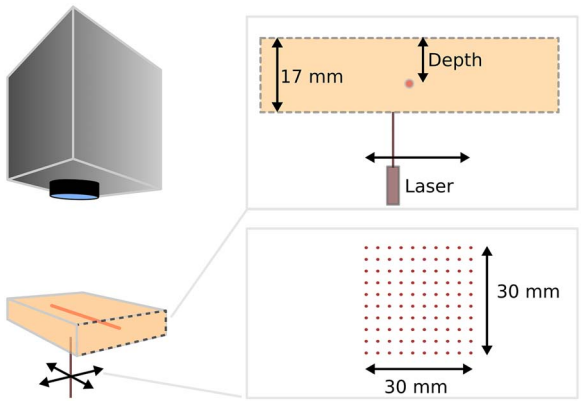

FIG. 1. (Color online) Schematic of the FDOT system. The phantom is scanned by a laser in a $30 \times 30\ \mathrm{mm}^2$ quadratic pattern from below. A CCD camera is used to capture an image for every scanned position. Upper right shows a cross section of the phantom, with the depth defined from the top surface to the center of the fluorescent capillary tube.

Figure 2 shows the reconstructions using Rhodamine 6G and the upconverting nanoparticles along with their respective projection errors. It can be seen that despite similar projection errors for the two cases, the Rhodamine 6G, which is affected by the intrinsic autofluorescence from the gelatin phantom, shows very severe artifacts especially at the two ends of the target. The reconstruction for the nanoparticles does not display such a behavior, indicating that the artifacts originate from the background autofluorescence. As mentioned above, since the problem is generally ill-conditioned, even relatively low amount of background perturbations can cause severe artifacts in the reconstructed results. In order to rule out model mismatches and further emphasize the differences between the two reconstructions, cross-sectional slices of the reconstructed relative fluorophore distributions are shown in Fig. 3. For both reconstructions, the true depth is relatively well reconstructed at the center of the fluorescent target. However, at the two ends of the target, the reconstruc-

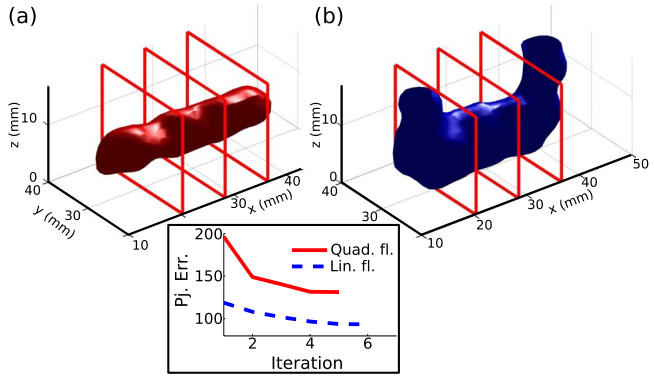

FIG. 2. (Color online) Three-dimensional rendering of the reconstructed fluorophores. The boxes indicate the positions of the cross-sectional slices shown in Fig. 3. (a) Reconstruction using upconverting nanoparticles shows a uniform and confined fluorophore distribution. (b) Reconstruction using Rhodamine 6G shows severe artifacts at the two ends of the fluorescent target. The inset shows the projection errors for the reconstructions as a function of iteration number.

tion of Rhodamine 6G is far from satisfactory, showing inhomogeneous distribution of the dye with severe spatial artifacts. The reconstruction for the nanoparticles, on the other hand, shows exceptionally good contrast and relatively homogeneous distribution across the whole reconstructed region with only minor spatial artifacts. The artifacts are most likely caused by small experimental mismatches of the coupling constants. Furthermore, an interesting effect is that the reconstructed target is much more confined for the case of nanoparticles, i.e., the reconstructed target appears less diffuse. It is also worth to mention that the transillumination setup used in this study is considered to be much less sensitive to autofluorescence than an epi-fluorescence setup.

As seen from the results presented in this letter, the tomographic reconstruction of the autofluorescence-insensitive nanoparticles is of higher quality than the reconstruction of the Stokes-shifting dye even in a weakly autofluorescent background. All reconstructed results presented show the relative concentrations. However, with pre-experimental calibrations, absolute reconstructions can be retrieved. This step was omitted in this work since the spatial shape of a reconstruction is not altered upon quantitative calibration. Although the reduced artifacts in the results for the nanoparticles can be explained by the lack of autofluorescence, we,

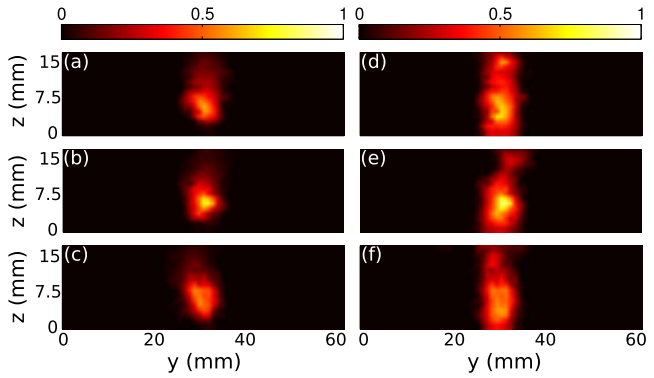

FIG. 3. (Color online) Cross-sectional slices of the reconstructed relative nanoparticle and Rhodamine 6G distributions. (a), (b), and (c) show slices at positions $x=20$, 28, and 36 mm for the nanoparticles. (d), (e), and (f) show slices at positions $x=20$, 28, and 36 mm for Rhodamine 6G.

however, do not believe that this can solely explain the effect of better confined reconstructions. We believe that the enhancement of the confinement is due to the more narrow sensitivity profiles with the use of the quadratic source term as seen in, for example, Eq. (4). This can be visualized by considering the collected signal for different source positions. Using a quadratic fluorophore, the signal will only be strong if the source position is in the vicinity of the fluorophore itself. Thus the signal is more sensitive to the location of the fluorophore than for the case of a linear fluorophore. This may also give the possibility of resolving, for example, two closely situated fluorophores that are not resolvable using a linear fluorophore. Preliminary simulations support these points. In addition, the simulations also show that the differences in optical properties for the two fluorophores can be dismissed and is not the main contributor to the enhanced confinement effect. Future work is planned to investigate this further.

In summary, we have developed a method for FDOT, which employs nonlinear upconverting nanoparticles. Due to the exceptionally good signal-to-background contrast obtainable using upconverting nanoparticles, reconstruction artifacts that commonly plague Stokes-shifting fluorophores can be effectively suppressed. Furthermore, the nonlinear power-dependent upconverting process leads to more sharply defined reconstructions of the fluorophore distribution, and also opens the possibility to resolve two closely situated fluorophores which cannot be resolved using linear fluorophores.

The authors gratefully acknowledge Professor Zhiguo Zhang and his group of Harbin Institute of Technology and Dr. Gabriel Somesfalean for the generous donation of the upconverting nanoparticles within an ongoing collaboration. This work was supported by Swedish Research Council Grant No. VR 2007-4214.

[1]G. D. Luker and K. E. Luker, J. Nucl. Med. **49**, 1 (2007).
[2]V. Ntziachristos, Annu. Rev. Biomed. Eng. **8**, 1 (2006).
[3]M. Yang, E. Baranov, X. M. Li, J. W. Wang, P. Jiang, L. Li, A. R. Moossa, S. Penman, and R. M. Hoffman, Proc. Natl. Acad. Sci. U.S.A. **98**, 2616 (2001).
[4]A. H. Hielscher, Curr. Opin. Biotechnol. **16**, 79 (2005).
[5]G. Y. Panasyuk, Z. M. Wang, J. C. Schotland, and V. A. Markel, Opt. Lett. **33**, 1744 (2008).
[6]D. C. Comsa, T. J. Farrell, and M. S. Patterson, Phys. Med. Biol. **53**, 5797 (2008).
[7]J. R. Mansfield, K. W. Gossage, C. C. Hoyt, and R. M. Levenson, J. Biomed. Opt. **10**, 041207 (2005).
[8]E. Tholouli, F. Sweeney, E. Barrow, V. Clay, J. A. Hoyland, and R. J. Byers, J. Pathol. **216**, 275 (2008).
[9]S. Heer, K. Kompe, H. Güdel, and M. Haase, Adv. Mater. (Weinheim, Ger.) **16**, 2102 (2004).
[10]G. S. Yi and G. M. Chow, Chem. Mater. **19**, 341 (2007).
[11]G. Y. Chen, H. C. Liu, G. Somesfalean, Y. Q. Sheng, H. J. Liang, Z. G. Zhang, Q. Sun, and F. P. Wang, Appl. Phys. Lett. **92**, 113114 (2008).
[12]C. Salthouse, S. Hildebrand, R. Weissleder, and U. Mahmood, Opt. Express **16**, 21731 (2008).
[13]C. T. Xu, N. Svensson, J. Axelsson, P. Svenmarker, G. Somesfalean, G. Chen, H. Liang, H. Liu, Z. Zhang, and S. Andersson-Engels, Appl. Phys. Lett. **93**, 171103 (2008).
[14]E. Alerstam, S. Andersson-Engels, and T. Svensson, J. Biomed. Opt. **13**, 041304 (2008).
[15]G. Alexandrakis, F. R. Rannou, and A. F. Chatziioannou, Phys. Med. Biol. **50**, 4225 (2005).
[16]B. Ballou, B. Lagerholm, L. Ernst, M. Bruchez, and A. Waggoner, Bioconjugate Chem. **15**, 79 (2004).